Earth's Future

RESEARCH ARTICLE
10.1029/2023EF004172

Response of Land Surface Albedo to Fire Disturbance in the Sierra Nevada Seasonal Snow Zone Over the MODIS Record

J. M. Gayler[1] and **S. M. Skiles**[1]

[1]University of Utah, Salt Lake City, UT, USA

Key Points:

- Land surface albedo response to fire in the Sierra Nevada seasonal snow zone varies with snow cover, land characteristics, and burn severity
- Contrary to current understanding, post-fire snow-free dates were variable and not consistently earlier than in surrounding unburned areas
- Fire-induced albedo changes led to greater cooling effect (net negative radiative forcing) in moderate compared to high-burn severity areas

Correspondence to:
J. M. Gayler and S. M. Skiles,
jillian.gayler@utah.edu;
m.skiles@utah.edu

Citation:
Gayler, J. M., & Skiles, S. M. (2024). Response of land surface albedo to fire disturbance in the Sierra Nevada seasonal snow zone over the MODIS record. *Earth's Future*, *12*, e2023EF004172. https://doi.org/10.1029/2023EF004172

Received 16 OCT 2023
Accepted 2 MAY 2024

Abstract Wildfires in the snow zone can brighten winter and spring landscapes by removing forest canopy, revealing underlying snow cover. Land surface albedo (LSA) alterations associated with transitioning from a canopied, snow-hiding vegetation regime to a snow-revealing landscape have impacts on the surface energy balance, with implications for climate and water supply. Forest fires are increasing in frequency, size, and elevation, but the change in LSA due to fire in the seasonal snow zone (SSZ) is poorly understood. This study addresses this knowledge gap for the Sierra Nevada, where recent climatic changes have contributed to droughts, earlier and more rapidly declining snowpacks, and worsening wildfire impacts. Remotely sensed snow fraction and LSA data from Moderate Resolution Imaging Spectrometer were used to assess the impact of wildfire on landscapes in the Sierra Nevada SSZ by comparing LSA in burn scars to unburned control areas and the historical average LSA, then quantifying the surface radiative forcing (RF) associated with change in LSA. Among high and moderate burn severity fires, winter LSA varied depending on snow cover, land characteristics, and burn severity, ranging from 0.12 in low-snow fire scars to 0.47 in snow-covered fire scars. This study adds to understanding of how landscapes respond to wildfires and the subsequent impacts on the surface energy balance.

Plain Language Summary Wildfires alter how the landscape absorbs and reflects sunlight by removing forest canopy and exposing the underlying ground surface, leading to changes in surface temperature. This impact is particularly pronounced in areas that are snow-covered due to the brightness of snow contrasted with dark canopy. As wildfires become more frequent, intense, and larger, it is crucial to understand how they affect seasonally snow-covered landscapes. This study focuses on the Sierra Nevada, CA, where recent climate changes have led to more droughts, earlier melting of snow, and intensifying wildfire. We used satellite data to study how wildfires impact landscape reflectance by comparing burned areas to both nearby unburned areas and historical data. We found that great variability was present in landscape response but overall, in the first 4 years after a high or moderate severity wildfire, the snow-covered areas were brighter in winter compared to unburned areas. Quantifying how absorption of sunlight changes following wildfire helps us understand how landscapes respond to wildfires and how they affect the local climate.

1. Introduction

Wildfire frequency and intensity are increasing across the western United States (Abatzoglou & Williams, 2016; Dennison et al., 2014; Ghimire et al., 2012; Westerling, 2016; Westerling et al., 2006; Williams & Abatzoglou, 2016; Williams et al., 2022), a trend particularly evident in the California Sierra Nevada (Schwartz et al., 2015; Williams et al., 2019). The increase in wildfires in the mountains of the Western US has been driven by climatic factors including rising temperatures, drier summers, below-average winter precipitation, and earlier spring snowmelt (Littell et al., 2009; Morgan et al., 2008; Westerling, 2016; Westerling et al., 2006). Wildfire potential in the Sierra Nevada is extremely susceptible to climatic changes, with a 1°C increase in daily summer temperature causing a 19%–22% increase in likelihood of fire occurrence and 22%–25% increase in area burned (Gutierrez et al., 2021).

Hydrology in the Sierra Nevada is dominated by snowmelt; trends in snow cover and melt timing are particularly relevant contributors to wildfire potential (Bales et al., 2011; Harpold et al., 2015; Li et al., 2017; Miller & Urban, 1999). Declining spring snow storage, earlier melt onset, and reduced streamflow have been attributed to climate warming, and trends are expected to continue through the 21st century with direct implications for fire frequency and intensity, including in the Sierra Nevada (Gergel et al., 2017; Westerling et al., 2006). Studies suggest wildfires that burn at elevations where most precipitation falls as snow, referred to as the SSZ, in turn

exert important controls on snow patterns in the Sierra Nevada for years after fire occurrence (Alizadeh et al., 2021; Gleason et al., 2019; Hatchett, 2021). Fire alters snow accumulation and ablation patterns through reduction of canopy snow interception, increased transmission of solar radiation to the snowpack surface, and deposition of light-absorbing particles (LAPs) in the form of black carbon and charred woody debris (CWD) on the snow surface (Boon, 2009; Burles & Boon, 2011; Gleason et al., 2013; Gleason & Nolin, 2016; Liu et al., 2005; Uecker et al., 2020; Winkler, 2011).

Also, wildfires that burn into the SSZ and remove forest canopy impact the broader surface energy balance largely by exposing snow and perturbing the landscape albedo, the ratio of reflected to incoming solar radiation. Snow is significantly brighter than the forest canopy, reflecting the majority of incoming sunlight; the albedo of newly fallen snow can range from 0.90 to 0.95, and can decrease to ~0.6 for aged melting snow (Wiscombe & Warren, 1980). In contrast, the albedo of Sierra Nevada snow-free forests is 0.10–0.13 (Barnes & Roy, 2010; Rother et al., 2022). Albedo of forested landscapes blanketed in snow can be more reflective, from 0.15 to 0.24, depending on the presence of canopy snow. Albedo in snow-covered treeless meadows, however, can be as high as 0.80 (Barnes & Roy, 2010; Burakowski et al., 2015; Pomeroy & Dion, 1996; Robinson & Kukla, 1984). The canopy masks the underlying snowpack from solar radiation, but when the canopy is removed due to disturbances such as wildfire, the forest stand energy balance changes to more closely resemble an open, unforested area. Even when snow is not present, the exposed underlying ground cover is typically brighter than the tree canopy, leading to a post-fire increase in albedo in coniferous forests (Veraverbeke et al., 2012).

Though wildfires deposit LAPs on the snow surface, decreasing the snow albedo, the overall land surface albedo (LSA) has been shown to increase in burned snow-covered forest stands in Wyoming (Gersh, et al., 2022). Impacts, though, are not well understood in the Sierra Nevada as burn severity, pre-fire vegetation structure, soil moisture, char deposition, and post-fire precipitation and vegetation recovery all contribute to the degree of change in LSA (Jin & Roy, 2005; Rother & De Sales, 2021). Increases in LSA due to land cover characteristics changing from snow-hiding to snow-revealing result in decreases in surface radiative forcing (RF), contributing to a climate-cooling effect (Barnes & Roy, 2010; Betts, 2000; Euskirchen et al., 2009), but to date this effect has not been quantified in the Sierra Nevada SSZ.

Here, changes in LSA and surface RF due to wildfire are quantified for six fires that have burned partially or fully in the Sierra Nevada SSZ. This fills a gap in previous studies that have used field methods and remote sensing sources to focus on impacts of wildfire on plot-to landscape-scale snow cover and albedo (Burles & Boon, 2011; Gleason et al., 2013, 2019; Harpold et al., 2013; Micheletty et al., 2014) or remote sensing-derived landscape-scale LSA changes in snow-off periods (Rother & De Sales, 2021; Rother et al., 2022; Shrestha et al., 2022; Veraverbeke et al., 2012; Vlassova et al., 2014), leaving an incomplete understanding of the impacts of wildfire on the SSZ. The analysis leveraged over 20 years of data from Moderate Resolution Imaging Spectrometer (MODIS), including LSA and snow-covered fraction (SCF), to quantify the post-fire change in LSA and surface RF. Post-fire changes in LSA are increasingly important to understand in the Sierra Nevada as fire intensity, frequency, and impact in the mountain west are predicted to worsen (Barbero et al., 2015; Westerling et al., 2011).

2. Study Area and Data

2.1. Study Area

The Sierra Nevada extends over 450 miles between the latitudes of 40.5°N and 35.6°N. The region is dominated by high interannual precipitation and temperature variability, with 60%–80% of precipitation falling as snow in the winter. The area used in analysis consists of the SSZ in 10 watersheds (HUC 8) over the western slope of the Sierra Nevada (Figure 1), spanning 5,000–8,000 feet in elevation. The SSZ is defined, for this study, as pixels with greater than 50% snow cover between January 1 and April 1 over the MODIS record (2001–2022).

Six fires that burned into the SSZ were selected for analysis due to meeting the following criteria: (a) at least 25 MODIS pixels within the overlap between the fire scar and SSZ and (b) at least 10 years of record pre-fire (Table 1). Due to the length restriction of the MODIS data sets, most of these (five) occurred after 2012. As one exception we included the McNally fire that burned early in the record (2002). We made the exception due to the overlap with the SSZ, but note that for this fire, there is only 2 years of pre-fire data from MODIS.

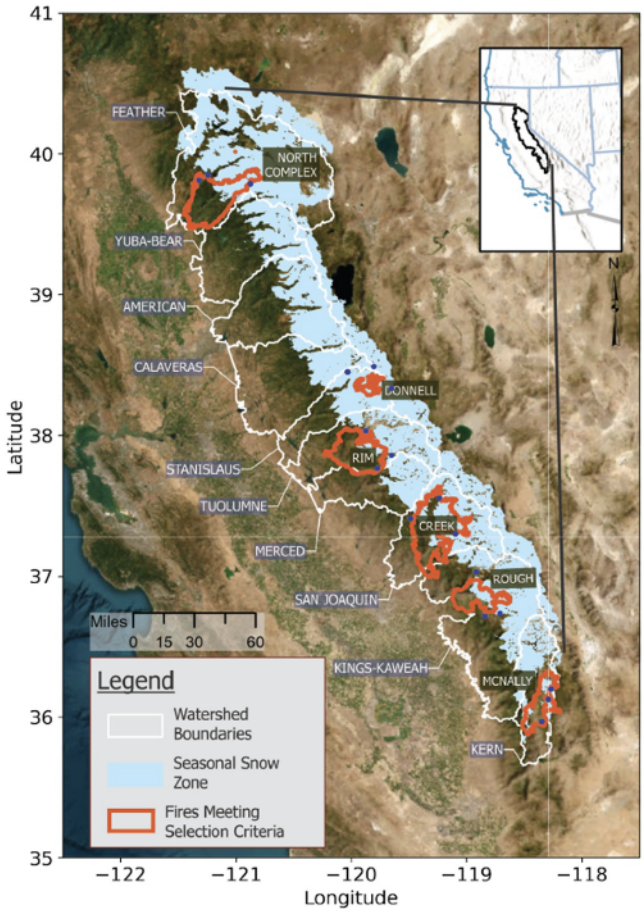

Figure 1. Sierra Nevada watershed boundaries outlined in white, seasonal snow zone shown in blue, the six analyzed fire boundaries shown in orange, and California Cooperative Snow Surveys site locations as blue dots.

2.2. Data

The LSA data set used in this analysis was sourced from the Moderate Resolution Imaging Spectrometer (MODIS) aboard the NASA satellite Terra. The MODIS sensor measures reflected solar radiation from the earth's surface every 1 to 2 days across 36 spectral bands; the first seven "land bands" are in the visible-shortwave infrared (VSWIR) range and have a spatial resolution of 500 m. The MODIS LSA product, MCD43A3 (Schaaf & Wang, 2021), provides 16-day averaged reflectance centered on the date of the satellite imagery overpass for each of the land bands, as well as in visible, near-infrared, and broadband ranges for directional hemispherical reflectance (black-sky albedo [BSA]) and bihemispherical reflectance (white-sky albedo [WSA]). The actual bidirectional reflectance albedo ("blue-sky" albedo) is a ratio of BSA and WSA; what we report as LSA is a simple 1:1 ratio of BSA to WSA (French et al., 2016).

The SCF data set, also sourced from MODIS-Terra, was generated using the Snow Cover and Grain Size (MODSCAG) algorithm. MODSCAG retrieves per-pixel SCF by applying spectral mixture analysis (SMA) to VSWIR surface reflectance (MOD09GA) (Painter et al., 2009). The SMA workflow is based on a set of linear equations that solve for subpixel fraction of clean snow (over a wide range of grain sizes), shade, vegetation, rock, and other surface covers. To address challenges in mapping "non-viewable" snow cover in dense canopy cover, MODSCAG interpolates viewable snow fraction that is canopy-adjusted (Rittger et al., 2020). The canopy adjustment corrects for the masking effects of vegetation at off nadir viewing angles and is based on canopy height and coincident per pixel vegetation fraction (Rittger, et al., 2020). The lower limit of snow detection has not been quantified; and traditionally 15% has been used as threshold below which SCF becomes less reliable (Painter et al., 2009). For this analysis we used the spatially and temporally complete (STC) version of MODSCAG, which gap fills the canopy corrected SCF through space and time to produce a daily product (Rittger et al., 2021). Compared to high resolution snow cover delineated from lidar mapped snow depths, including multiple watersheds in the Sierra Nevada, the bias (−0.1%), root mean squared error (12%), and F statistic (95.6) indicates improved performance relative to band-ratio based snow cover products (i.e., MOD10A1) (Stillinger et al., 2023). The comparison also showed that MODSCAG-STC underestimates SCF at high snow extents whereas it overestimates SCF at low snow extents and in dense canopies (Stillinger et al., 2023).

Data on burn area and severity were obtained from Monitoring Trends in Burn Severity (MTBS), an interagency program managed by the U.S. Geological Survey Center for Earth Resources Observation and Science and the United States Forest Service (USFS) Geospatial Technology and Applications Center (GTAC) (Eidenshink et al., 2007). The MTBS products leverage Landsat 30-meter spatial resolution data and data from similar sensors to generate burn severity maps. To determine burn severity, a Normalized Burn Ratio (NBR) was generated from reflectance in the near-infrared spectral range (Landsat band TM4) and the shortwave infrared spectral range (Landsat band TM7) for scenes pre- and post-fire (Key & Benson, 2005). Subtracting the post-fire NBR from the pre-fire NBR results in a differenced NBR (dNBR) and dividing dNBR by the pre-fire NBR results in a relativized dNBR (RdNBR) (Miller & Thode, 2007). Both dNBR and RdNBR are used to classify each pixel into one of five classifications: unburned, unburned to low, low, moderate, and high. For this study, the MTBS data was resampled to MODIS resolution using a modal resampling method.

Ecoregion, tree cover, and forest type land cover data sets were used to help understand characteristics of each pixel. Ecoregion boundaries were obtained from the U.S. Environmental Protection Agency Level IV Ecoregion map (Griffith et al., 2016). Forest type was sourced from the USFS GTAC and Forest Inventory and Analysis (FIA) National Forest Type Data set, which uses land characteristics and climate data to model forest type over the continental U.S (Ruefenacht et al., 2008). Tree cover data were obtained from the USFS GTAC and FIA Tree

Table 1
Characteristics of Burned Pixels in the SSZ From the Six Sierra Nevada Wildfires Analyzed in This Study and Characteristics of Unburned Pixels Used in Comparison

Watershed	Fire	Ignition year	Total burn area (ac)	Average elevation (ft)	Primary burn severity	Predominant ecoregion	Average 2011 tree cover (%)	Predominant forest type
Stanislaus	Donnell	2018	36,200	7,100	High	N.S. Upper montane forests	49	CA mixed conifer
	Unburned			7,000		N.S. Upper montane forests	48	CA mixed conifer
San Joaquin	Creek	2020	381,400	6,900	Low	S.S. Mid-Montane forests	47	CA mixed conifer
	Unburned			7,300		S.S. Mid-Montane forests	54	CA mixed conifer
Kern	McNally	2002	146,600	6,800	High	S.S. Mid-Montane forests		CA mixed conifer
	Unburned			7,300		S.S. Mid-Montane forests		CA mixed conifer
Kaweah	Rough	2015	146,400	6,100	Low	S.S. Lower Montane forest and woodland	51	CA mixed conifer
	Unburned			6,400		S.S. Lower Montane forest and woodland	53	CA mixed conifer
Tuolumne	Rim	2013	257,100	5,600	Low	S.S. Upper montane forests	30	CA mixed conifer
	Unburned			5,900		S.S. Upper montane forests	44	CA mixed conifer
Feather	North complex	2020	316,600	5,100	Low	N.S. Mid-Montane forests	56	CA mixed conifer
	Unburned			5,300		N.S. Mid-Montane forests	66	CA mixed conifer

Note. Burn area refers to the entire fire extent; all other characteristics are representative of only the overlapping area between fire scar and SSZ (N.S.: Northern Sierra; S.S.: Southern Sierra).

Canopy Cover (TCC) data set, which contains percent tree canopy estimates for each 30-m pixel across the continental U.S. as part of the National Land Cover Database (Coulston et al., 2012). We used the TCC data set from 2011 as it maps TCC prior to the occurrence of the analyzed fires (the McNally Fire occurred in 2002 and does not have pre-fire tree cover data). The ecoregion, forest type, and tree cover data sets were resampled to MODIS resolution using a modal resampling method for ecoregion and forest type, and a bilinear resampling method for tree cover.

3. Methods

3.1. Changes in Post-Fire LSA

To quantify changes from wildfire, LSA was quantified for the following three conditions: pre-fire in the burn scar, post-fire in the burn scar (LSA_b), and post-fire outside the burn scar (LSA_u). All data was masked to MODIS pixels within the SSZ. If burned, each pixel was classified as either moderate or high burn severity. The unburned pixels selected for comparison were within 1° latitude and longitude (~70 miles) from the fire scar, within the same watershed boundary, had greater than 40% tree cover, and had not been burned by any other fire within the previous 10 years. The pre-fire historical average LSA was calculated by averaging LSA in all moderate-to high-severity burned pixels within the fire scar for each calendar month over the years leading up to the ignition date. The McNally Fire (ignited 2002) was the only fire without at least 10 years of pre-fire record, so the historical average LSA was calculated over the 2 years pre-fire covered by the MODIS record.

The changes in LSA were then analyzed at the fire scar scale in two ways: first, the difference between LSA_b to LSA_u, and second, the difference between the pre-fire historical average LSA to LSA_b. Comparisons of each were made by calculating the mean LSA values for winter (December through February) and spring (March through May). We then analyzed a time series comparison between pre-fire monthly average LSA values, LSA_u, and LSA_b in the first 4 years following each fire. The SCF data were resampled to a 16-day weighted average to align with LSA.

3.2. Snow-Free Date Analysis

The snow-free date was defined as the day that the average LSA dropped below the snow-free threshold and remained there for over 7 days (Cox et al., 2017). This approach was adapted to MODIS based on methods in Stone et al. (2002) and Cox et al. (2017) that found LSA thresholds matched visual observations of snow disappearance in the tundra. The unburned threshold was calculated as the average post-fire July–August LSA in

unburned pixels and the burned threshold was calculated as the average post-fire July–August LSA in burned pixels. These months were selected because these are the months that were the most reliably snow free and LSA exhibits low variability. The LSA threshold was preferred relative to a SCF threshold because (a) SCF is biased high at low snow extents and in dense canopy cover, (b) the lower limit of SCF detection from MODSCAG-STC is not known, and (c) SCF is interpolated in the forests making the snow free determination dates in unburned areas less reliable. Additionally, LSA is the metric of interest for surface energy balance and using the LSA threshold makes the analysis self-consistent with the radiative forcing analysis (Section 3.3). Relatedly, we note that using an LSA threshold to define the snow-free date means that the snow-free date is different than the melt-out date—the melt-out date implies the total snowpack has ablated on that date, while the snow-free date refers to the date that snow is no longer sensed by MCD43A3 retrievals.

3.3. Surface Radiative Forcing

Changes in monthly LSA were then used in conjunction with at-surface downward shortwave radiation (DSR) to calculate the albedo-induced surface RF. We calculated RF using the equation:

$$RF = (LSA_b - LSA_u) * DSR$$

where LSA_b and LSA_u represent the LSA for burned and unburned areas, respectively. DSR was obtained from the NASA GeoNEX DSR/PAR product, which uses top of atmosphere reflectance to generate a physical-based look-up table for hourly at-surface DSR at 1 km resolution (Li et al., 2022), which we averaged into daily values and resampled to 500-m spatial resolution. For this analysis, a monthly average DSR value was calculated from the daily data, averaged over the available data record from January 2018 through December 2021 (Liu et al., 2005). This was used in conjunction with the monthly average LSA_b and LSA_u from the first 4 years post-fire to determine surface RF for high and moderate burn severity areas, respectively.

4. Results

4.1. Changes in LSA in a High Severity, High Elevation Fire

Generally, the results of the analysis showed that in seasons with widespread and long-lasting snow cover, wildfire in the SSZ can raise the LSA, brightening the landscape primarily by exposing snow cover. As a demonstration of this, we start by presenting results from the Donnell Fire in the Stanislaus Basin, which ignited in 2018 and burned 36,200 acres. Although not a large fire relative to the others in the data set, it was a high-intensity, high-elevation fire that burned fully in the SSZ, making it an interesting example and case study. Then we compare Donnell with the other larger fires, representing a broader range of elevations, land surface characteristics, and fire severity.

For the Donnell Fire, we found that LSA in the burned area was consistently higher than LSA in forested pixels outside the burn area, an impact that lasted for years following the fire. To visualize the change that snow exposure can have on LSA, high-resolution true color remote sensing imagery (Sentinel-2 L2A RGB) and LSA from post-fire snow-off and snow-on conditions were compared over a domain encompassing the fire scar (Figure 2). The fire scar is visible in the snow-off date (Aug 25) contrasting with the darker, vegetated unburned area; correspondingly, for pixels in the burn scar that previously had a relatively high tree cover fraction, the LSA is higher relative to similar pixels outside the burn scar (Table 2). The LSA is higher still in unburned pixels with low vegetation fraction, demonstrating the important control that tree cover has on LSA. The important role of snow exposure and canopy removal on LSA is apparent in the snow-on image (March 18), even though the fire scar itself is less obvious in the imagery. The burn area pixels have a much higher LSA than the unburned forested area even though the SCF is lower, due to greater exposure of snow that is present (Table 2). The LSA remains highest in the nearby pixels with low tree cover, where exposed snow extent is highest (Table 2).

Comparing all burned pixels in the SSZ to those outside of the fire scar, the Donnell Fire showed a significant increase in winter and spring LSA. In the winter following the Donnell fire, the average LSA_b was 0.47 (±0.13) and the average LSA_u in forested pixels was 0.40 (±0.06), a ~18% increase. In the spring the average LSA_b was 0.46 (s ± 0.10) and the average forested LSA_u was 0.36 (±0.08), a ~28% increase. Burned and unburned LSA varied annually with respect to the historical average, but the LSA_b was consistently greater than the LSA_u in the

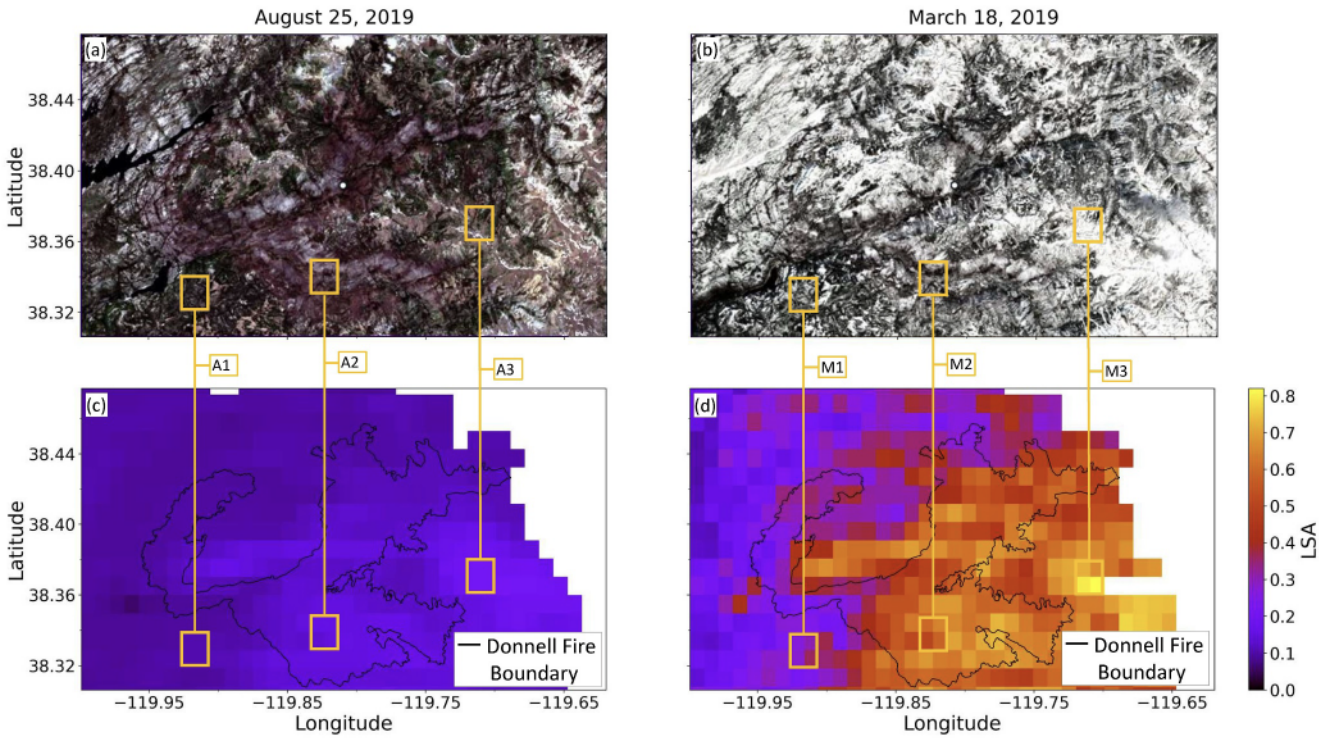

Figure 2. Satellite imagery (Sentinel-2 L2A RGB) of the Donnell Fire in (a) snow-off and (b) snow-on conditions and the land surface albedo (LSA) map for the same (c) snow-off and (d) snow-on days, with the Donnell Fire outlined. Corresponding areas are shown in connecting boxes, and characteristics for each labeled box pair (e.g., A1, M1) are summarized in Table 2 for reference. The LSA maps are 16-day averages centered on the date of the satellite imagery overpass.

first four years-post fire (Figure 3). In the first year following the Donnell Fire, these increases led to the absorbed DSR in the burned area being 33% lower respective to pre-fire conditions in both winter and spring.

Seasonally, patterns in LSA_b and LSA_u in the Stanislaus Basin indicate changes are directly related to exposed snow cover in the Donnell Fire scar. Although both LSA_b and LSA_u increased in response to snow accumulation in November, LSA_b reached a higher magnitude and remained higher through the accumulation period (Figure 4). The increase in LSA_b relative to LSA_u was most notable when the basin was consistently snow-covered, as indicated by the SCF. During this period, from mid-February to early April, the LSA_b remained higher than LSA_u, but the albedo decay occurred at a similar rate.

The SCF in burned areas was consistently high through the winter and into the summer, well after SCF in unburned areas declined. Though the SCF in burned areas remained consistently high, change in snow cover is more apparent in the LSA_b time series, which fluctuated through the winter and spring in response to new snowfall. In the spring, LSA_b declined before SCF, showing that as expected, albedo decay preceded snowmelt.

Table 2
Land Cover Characteristics for Each of the Boxes Shown in Figure 2

	Burn classification	2011 tree cover (%)	Ecoregion	SCF (%)	LSA
A1	Unburned	50.5	Northern Sierra upper montane forests	0.0	0.10
A2	Burned—High severity	47.5	Northern Sierra upper montane forests	0.0	0.15
A3	Unburned	18.0	Northern Sierra subalpine forests	0.0	0.20
M1	Unburned	50.5	Northern Sierra upper montane forests	92.8	0.30
M2	Burned—High severity	47.5	Northern Sierra upper montane forests	87.6	0.58
M3	Unburned	18.0	Northern Sierra subalpine forests	94.3	0.75

Note. Tree cover data is from pre-fire conditions; all other variables represent characteristics on the shown date.

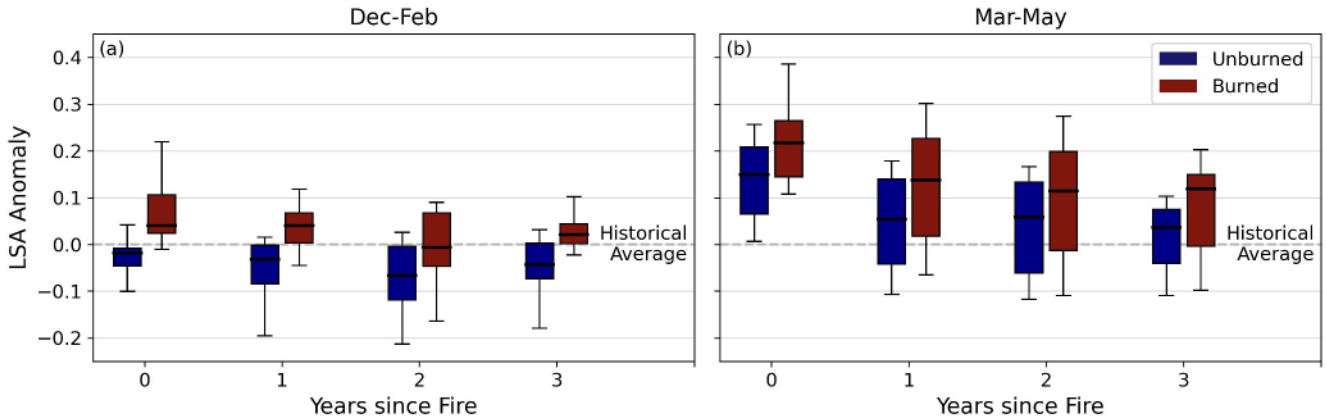

Figure 3. Donnell Fire (Stanislaus Basin) winter and spring LSA_b and LSA_u anomalies relative to the historical average, showing that both winter and spring LSA_b increases were significant for at least 4 years post-fire.

4.2. Snow-Free Dates

The landscape within the Donnell Fire burn scar had a later-than-average snow-free date than the surrounding unburned areas in each of the 4 years following the fire (Figure 5). The difference was greatest in the first spring post-fire when LSA_b reached the "snow-free" threshold 18 days after LSA_u. In the three subsequent years, the difference in snow-free dates was 14, 10, and 13 days, respectively. The LSA threshold was 0.14 for the burned area and 0.11 for the unburned area (pre- and post-fire), demonstrating that the snow-off LSA_b was significantly impacted by loss in forest canopy (p-value = 0.008) even in the absence of snow cover.

Expanding the analysis to include all other fires in the data set, which included both moderate and high severity pixels, results in three of six fires aligning more with the current understanding of wildfire impacts on melt-out dates: that the high severity pixels had an earlier average snow-free date than the surrounding unburned area (Table 3). The high severity fires that were the exception (the North Complex, McNally, and Donnell fires) as well as the variability in post-fire melt out dates across all fires indicate, though, that an earlier snow-free date is not consistently the outcome post-fire. For the three fires with moderate burn pixels there was also variability in snow-free date post-fire; two of the fires (Rough, Creek) had consistently earlier snow free dates while the McNally fire had both earlier and later snow free dates. To lend confidence to our assumption that unburned pixels

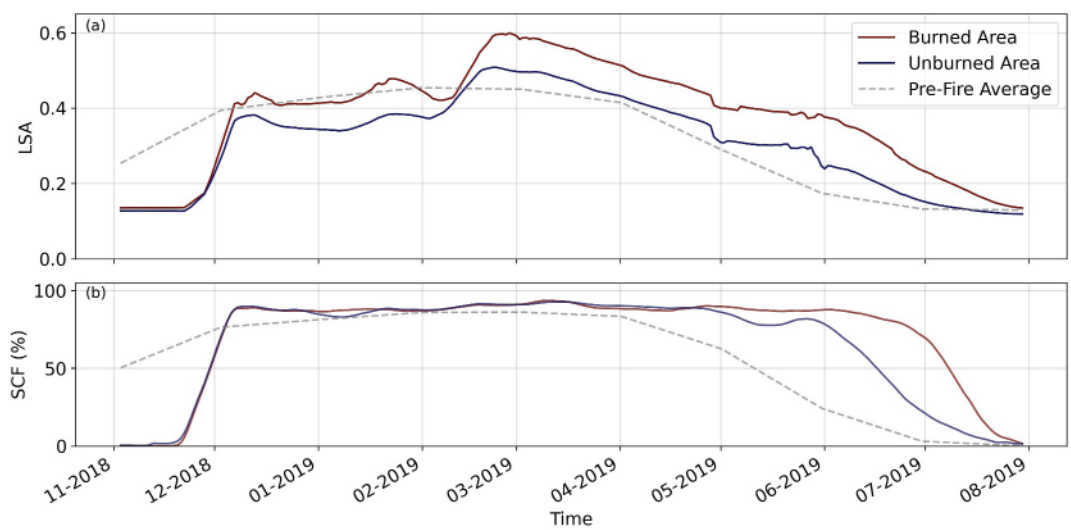

Figure 4. A time series of land surface albedo (LSA) and snow-covered fraction (SCF) following the Donnell Fire. Figure (a) shows a time series of LSA_b, LSA_u, and the historical average LSA (pre-fire within the burn scar) and (b) shows the SCF in the burned area and unburned area of the Stanislaus Basin for the 1 year following the Donnell Fire.

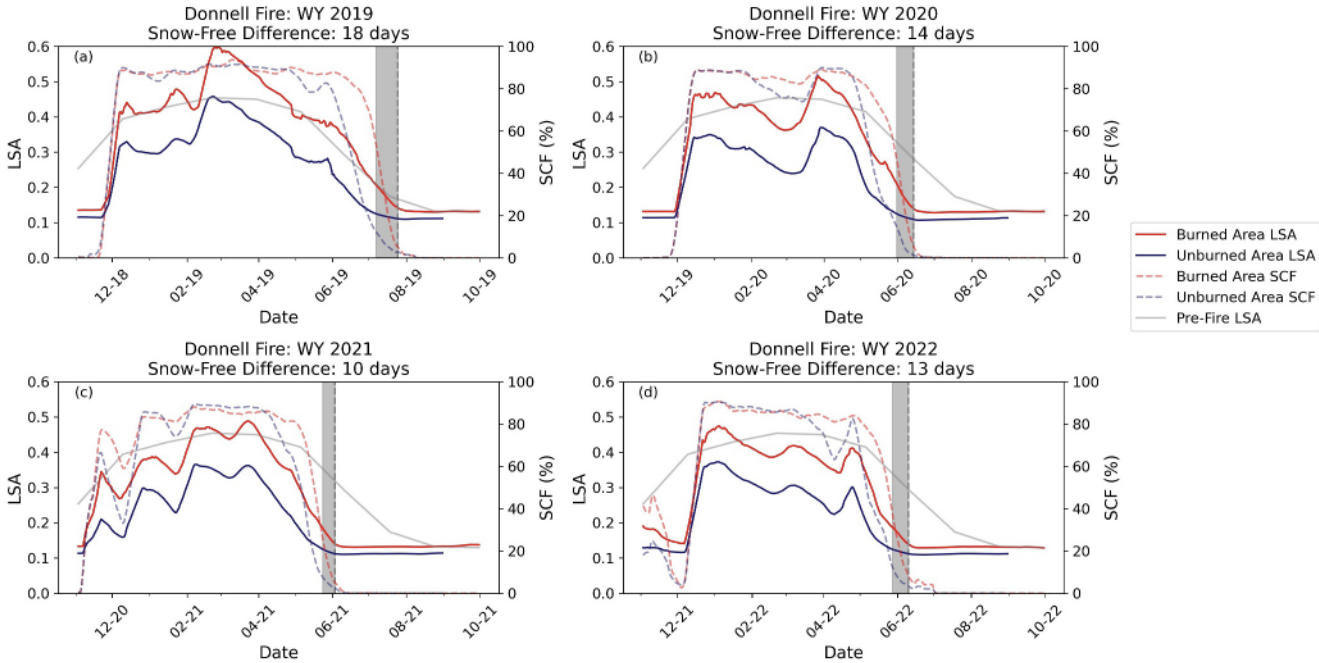

Figure 5. A time series of LSA_b, LSA_u, burned and unburned area snow-covered fraction, and the historical average land surface albedo for each of the 4 years following the Donnell Fire. Gray shading shows the difference in snow-free dates, with the dashed vertical line designating the burned area snow-free date.

are similar to pre-fire conditions, the LSA_u thresholds were compared against the average pre-fire snow-off LSA values and found to be within 0.005 for all basins.

4.3. LSA Changes by Fire and Burn Severity

Change in LSA following fire exhibited more variability across the other fires in the data set relative to the Donnell fire, which were all significantly larger with more variability in burn severity (Figure 6). The Donnell Fire exhibited the highest average December–February LSA_b, 0.47 ± 0.13, while the lowest winter LSA_b was 0.12 ± 0.05 in the Rim Fire. High burn severity LSA was consistently higher than LSA_u for the Rough Fire, but similar or lower in the Creek, Tuolumne, and North Complex Fires. Fires with moderate burned pixels in the SSZ (Creek, McNally, and Kaweah) showed higher magnitude LSA_b in the winter, but not consistently across the year.

Changes in LSA were heavily influenced by both snow cover and accumulated snow water equivalent (SWE), as well; droughts and low-snow periods occurred after the Creek Fire, North Complex Fire, and especially the Rim

Table 3
Change (Number of Days) in Snow-Free Date for Each Fire Scar, Showing the Four-Year Post-Fire Average and the Range of Minimum and Maximum Change Values Over the Four-Year Period

	Moderate		High	
Fire	Change in snow-free date (days)	LSA threshold	Change in snow-free date (days)	LSA threshold
Donnell			14 (+10/+18)	0.14 (±0.005)
Creek[a]	−14 (−15/−12)	0.10 (±0.004)	−26 (−36/−15)	0.10 (±0.002)
McNally	2 (−6/+8)	0.12 (±0.003)	4 (0/+11)	0.11 (±0.004)
Rough	−4 (−25/−6)	0.10 (±0.002)	−11 (−32/+32)	0.09 (±0.002)
Rim			−12 (−18/0)	0.10 (±0.004)
North Complex[a]			19 (+3/+34)	0.09 (±0.001)

Note. The change was calculated by subtracting the day of year that the control LSA_u returned to the unburned threshold from the day of year that the LSA_b returned to the burned threshold. [a]Fires that use 2 years of post-fire data.

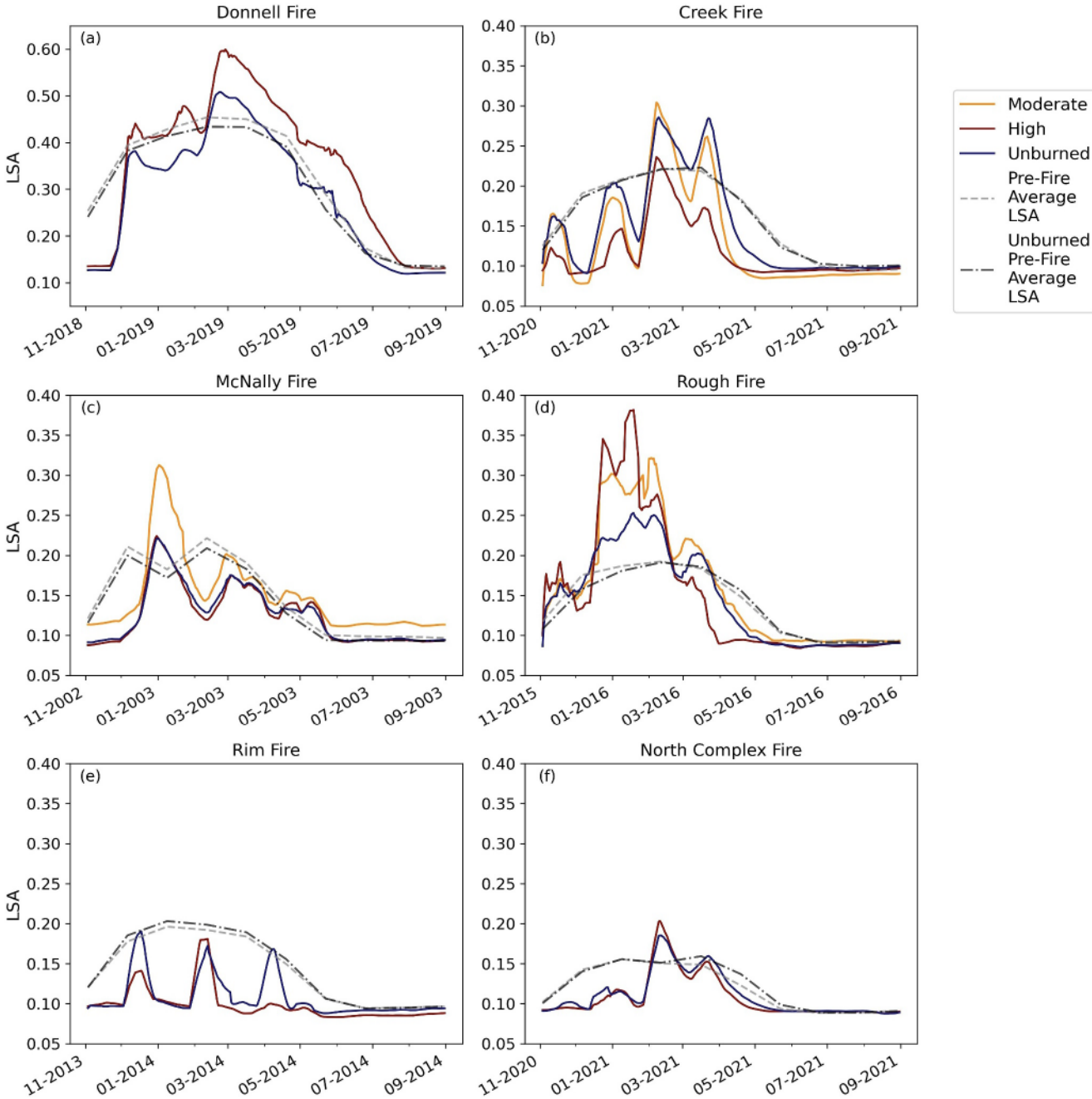

Figure 6. A time series of LSA_b for moderate and high severity burned pixels, LSA_u, and the historical average land surface albedo (LSA) for both burned and unburned areas. Values represent LSA inthe year immediately after each fire occurred.

Fire, while average to above-average snow years occurred after the Donnell Fire, McNally Fire, and Rough Fire (Figure 7). The Donnell Fire scar received more snow than the historical median and was more consistently covered in snow in the year after the fire. The Rim Fire, on the other extreme, received significantly below-average SWE and was consistently less snow-covered than years prior. The Creek Fire and the North Complex Fire showed lower than median SWE in the year post-fire, but no significant difference in median SCF. The McNally Fire received an above-average snowpack the year following the fire, but a similar median SCF to the historical median. The Rough Fire scar showed an average snowpack, with similar median and historical SCF.

10.1029/2023EF004172

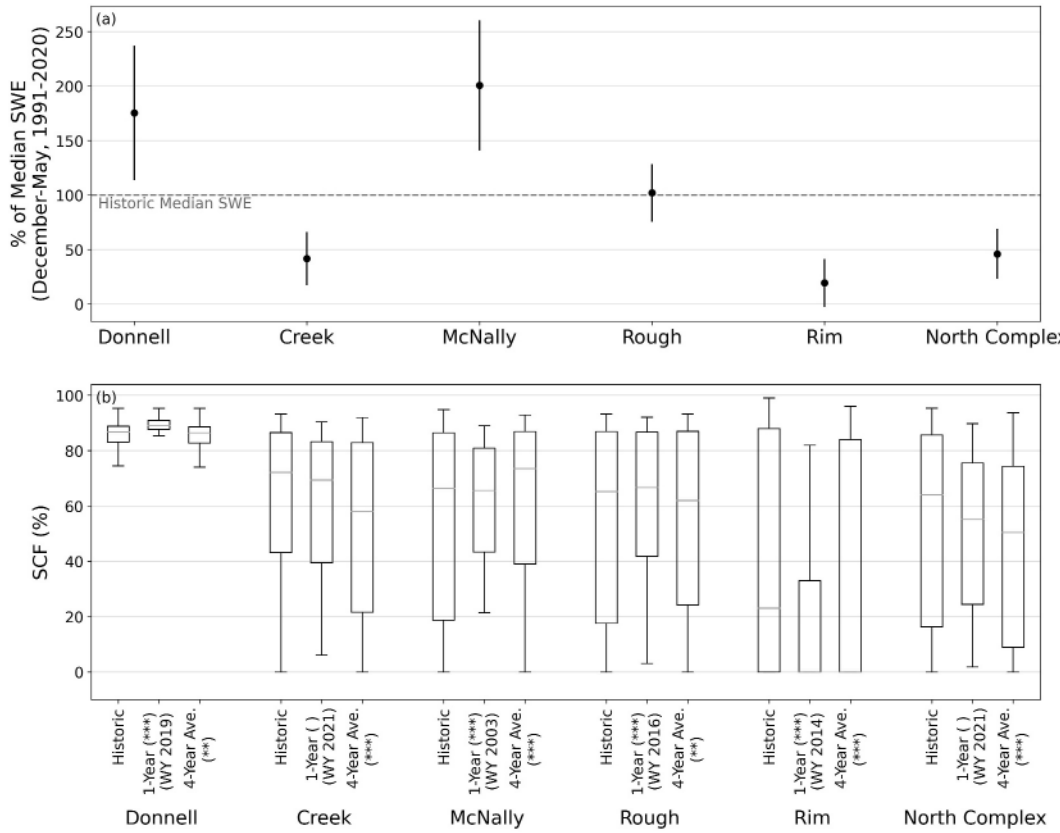

Figure 7. Comparisons of post-fire snow characteristics compared to historical values. (a) Shows the December–May percent of 1991–2020 median snow water equivalent for the First year post-fire with error bars representing one standard deviation. (b) Shows the December–May boxplots for historic, 1-year post-fire, and averaged 4-year post-fire snow-covered fraction. ** = p value < 0.01, *** = p value < 0.001 from Welch's t-test.

When grouped by fire severity, LSA anomalies over the first 4 years following fire occurrences (two for Creek and North Complex Fires) show that there is a large amount of variability in LSA changes compared to pre-fire conditions across burn severities and years following fire (Figure 8). In the winter, LSA in high- and moderate-severity burned pixels consistently increased from the historical average, while the LSA response in spring varied more. In the first 2 years post-fire, unburned, moderate-severity, and high-severity pixels all showed a negative anomaly. In the 3rd and 4th years following fire, the moderate-severity and high-severity burned pixels showed an increase over the respective historical averages, while the unburned pixel LSA was less than the historical average.

4.4. Surface Radiative Forcing

In most basins, the fire scar RF values grew increasingly negative in early winter, before increasing in the spring (Figure 9). In the first year following the consistently snow-covered Donnell Fire, this effect was more prolonged, leading to the most intense RF in the spring (average RF = -14.9 Wm^{-2}), when snow influence on LSA persisted in the burned area past the unburned area snow-free date, and less intense in winter (average RF = -10.1 Wm^{-2}). The 4-year post-fire average RF due to the Donnell Fire shows the largest RF values shifting earlier in the year to March and April. In the McNally Fire and Rough Fire scars, the 4-year post-fire average RF was greatest in December–February for moderate and high burn severity pixels. In the three fires with consistently low post-fire snow cover (Creek, Rim, North Complex Fires), the RF trended increasingly positive in late winter into spring, when darkened, charred forests and low snow cover likely contributed to the lower LSA_b, then minimized in the late spring into summer. The average December–February RF across all fires was -21.2 ± 86.4 Wm^{-2} and the average March–May RF was -16.0 ± 136 Wm^{-2}, exhibiting the broad range of fire impacts.

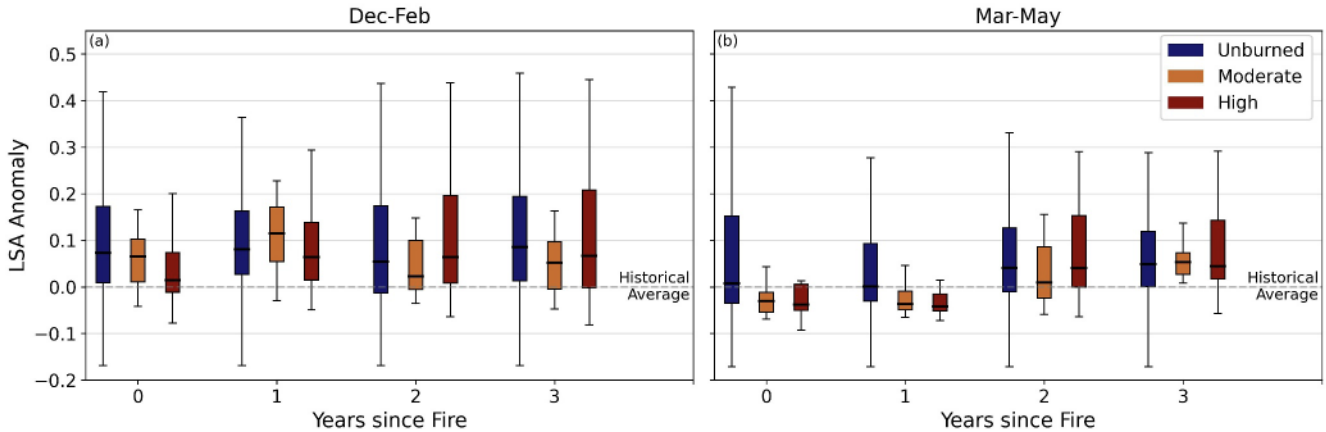

Figure 8. Seasonal land surface albedo (LSA) anomalies for unburned, moderate-severity burned, and high-severity burned pixels for each of the first 4 years post-fire. Anomalies were calculated as the difference from the historical average LSA for each burn regime.

Analyzing RF trends by burn severity reveals that the median RF in moderately burned pixels is consistently negative in the winter over the first 4 years (Figure 10). In the spring, moderate-severity burned pixels show minimal RF in the first 2 years. In both seasons, the RF magnitude is greater in the third and fourth years following the fire. In high-severity burned pixels, the median RF in the first 2 years is minimal or slightly positive, but also decreases in the proceeding years. Variability is greatest in high-severity burned pixels in the third and fourth years following fire.

5. Discussion

The LSA, a major driver of the surface energy balance, increased in fire scars with average to higher-than-average SWE and SCF during both snow-on and snow-off conditions. Considerable variability was present in the magnitude of change in LSA across fire scars, depending on timing after a fire, SWE, SCF, and fire severity. The Donnell Fire, an example of a high-elevation, high-burn severity fire followed by a significantly above-average snow year, showed that snow-on LSA can increase from 0.19–0.24 to 0.45–0.47 after a fire. In the Rim Fire scar, a relatively low-elevation fire followed by a historically low snow year led to decreases in LSA_b, indicating that post-fire LSA was dependent on post-fire snow presence as well as pre-fire drought conditions. Different results between these two extremes suggest that winter and spring LSA_b tend to increase more over LSA_u when there is substantial and widespread snowfall, which adds to the evidence that snow cover plays a major role in the surface energy balance. More work is needed to understand this relationship and to determine if there is a threshold of snow cover at which winter LSA_b is greater than LSA_u, below which LSA is driven by variables other than snow cover such as deposition of LAPs and CWD and ensuing feedbacks that accelerate snow darkening. Additionally, the differences between annual SWE and SCF anomalies, particularly for the Creek Fire and the McNally Fire, reinforce that SCF is not a proxy for snow accumulation, and further work needs to be done to understand how changes in snow albedo between storms may impact LSA.

The Donnell Fire scar snow-free date was, on average, 14 days later than the unburned area. The moderate burn severity pixels in the McNally Fire also showed a later snow-free date. This potentially indicates that for these areas, snow cover depleted faster in unburned, open areas than in areas that were open due to fire. This could be due to higher accumulation in burned areas, improved detectability of exposed snow cover, or a combination of the two. Independent of the reason for a later snow-free date, the result is still an increase in LSA over a longer period relative to nearby unburned areas. Previous research has shown that snow ablates earlier in burned areas compared to control unburned areas (Gleason et al., 2013; Kampf et al., 2022; McGrath et al., 2023) in studies using field observations and MOD10A1 SCF to determine a melt-out date. Our results largely agree with these results, but we argue snow depletion date alone does not tell the whole story. By using changes in LSA we were able to show that even when snow ablates earlier than surrounding unburned areas, the removal of canopy and exposure of brighter snow over the winter season can exert important controls on surface energy balance. By using different metrics to look at the entire system, instead of only snow ablation dates, results presented here add to the greater picture of fire impacts on the SSZ landscape.

10.1029/2023EF004172

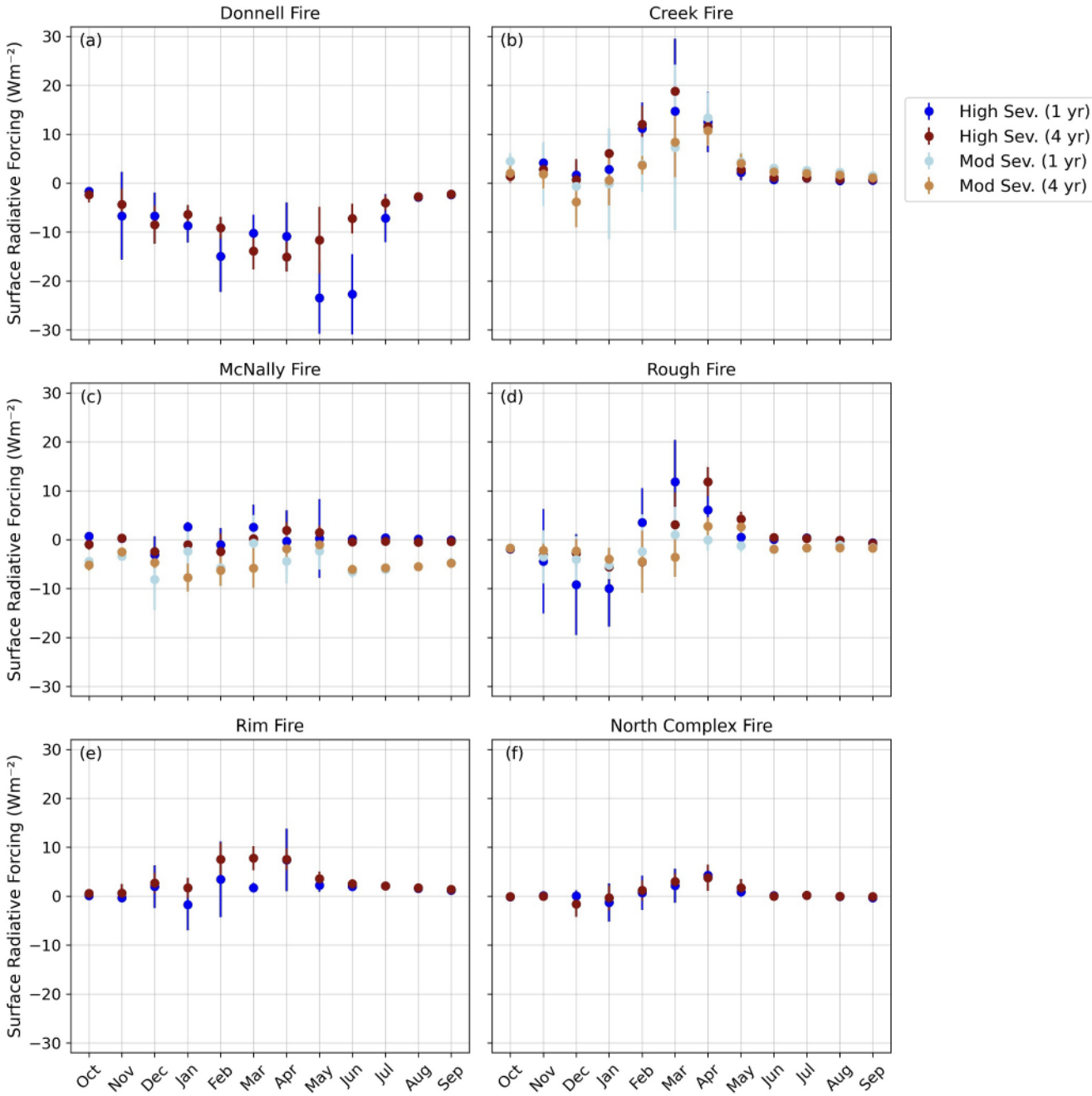

Figure 9. Monthly RF values for 1 year post-fire and averaged over 4 years post-fire. Error bars show one standard deviation.

Increases in LSA contributed to negative RF in fire scars with above-average post-fire snowpacks. Elevated RF values in these fire scars suggest that removing tree canopy and increasing underlying snow exposure led to an increase in reflected shortwave radiation, which, combined with a later snow-free date in burned areas and a higher snow-off LSA_b, may contribute to a localized cooling effect in burned areas. These results reflect the findings of past research in the US and in boreal forests that transitioning from a snow-hiding to a snow-revealing land surface increases albedo and decreases surface RF (Barnes & Roy, 2010; Betts, 2000). Climatic changes are causing snow to melt earlier in the spring across the Western US, potentially creating a snow/albedo feedback loop where LSA declines earlier, the landscape absorbs more solar radiation, and more energy is transferred to the atmosphere, a process that reinforces local warming. In burned, snow-revealing forests, more negative surface RF may have the opposite effect. However, LAPs

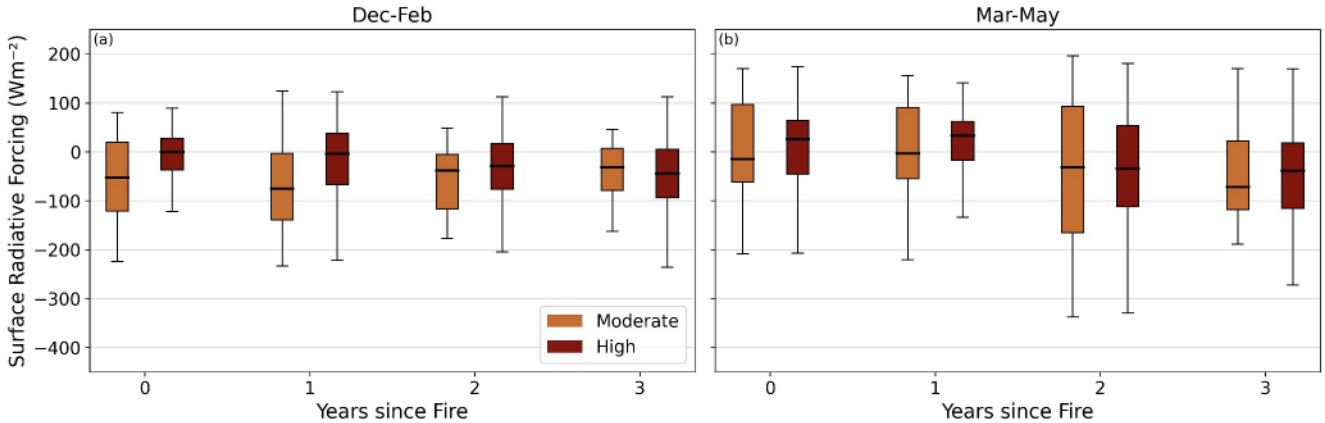

Figure 10. Seasonal RF due to change in land surface albedo from unburned to burned area for each of the first 4 years post-fire. Pixels are grouped by moderate and high burn severity.

distributed across snow in burned areas also increase the solar forcing compared to clean snow (Gleason et al., 2019), although LAP darkened snow is still likely brighter than the underlying land surface; the links between increasing LSA_b and decreasing snow albedo have yet to be explored.

The change in LSA associated with vegetation disturbance and subsequent snow exposure can alter the landscape's absorption of solar radiation. Ensuing RF may result in a cooling effect in post-fire Western US forests in addition to surface energy flux alterations due to the removal of vegetation (Bonan et al., 1992, 1995). These variables are important factors in climate models that seek to describe mesoscale and regional weather, snowmelt timing and rates, soil moisture, evapotranspiration rates, and potentially ocean circulation patterns (Andrews et al., 2017; Pielke et al., 2011). However, most hydrologic models and land surface models do not accurately incorporate post-fire LSA changes, leading to uncertainty in results (Koshkin et al., 2022). Here, uncertainty in LSA changes was likely heightened by noise associated with small sample sizes, a consequence of coarse spatial resolution MODIS pixels combined with fires that burned predominantly at low severity in the SSZ. However, the MODIS record is currently the best available data set and enables landscape-scale analysis, an important component of climate and energy balance models.

6. Conclusions

LSA is an important component of the surface energy balance; changes in LSA can lead to striking changes in local climate. Both wildfire and snow affect LSA, but the interactions between the two and their impact on fire scar-scale LSA have not previously been fully explored. In this study, we investigated the impact of wildfire on LSA in the Sierra Nevada SSZ using MODIS remote sensing data. We analyzed LSA, SCF, burn severities, and land surface characteristics to form a greater understanding of how LSA changes in fire scars and the greater impacts on surface RF. Our results suggest that (a) winter and spring LSA response to fire varied within the SSZ; (b) the magnitude of the change was influenced by burn severity, SCF, land characteristics, and climate conditions, with the largest increases in LSA found in the high-elevation, high-burn severity, and extensively snow-covered Donnell Fire scars; (c) post-fire snow-free dates varied considerably and fire, in some cases, delayed the snow-free date; and (d) RF associated with fire scar-scale changed in LSA was generally more negative in moderately burned pixels than high-severity burned pixels.

The Donnell Fire results show that in a high severity, high elevation fire, changes in LSA are particularly strong. Results across all fires were more varied and were highly influenced by snow cover. Further research is needed to understand how the SCF, frequency of storms, and snow accumulation affect LSA changes over time. Using MODIS SCF products is limiting due to less accurate snow detection under forest canopy and less accuracy at low SCF, but there is potential for improvement in understanding with future remote sensing missions.

The implications of this work are far-ranging, from incorporating albedo feedbacks into climate models to improving basin-scale runoff forecasting. As climate warming continues, we will likely continue to see wildfires impacting the SSZ, coincident with declines in seasonal snow, particularly in the Western US. Studying how these snow and wildfire processes interact is critical to prepare for changing climate impacts on mountain eco- and hydrologic systems.

Data Availability Statement

The MODIS LSA data (MCD43A3 v061) are freely available from NASA-LPDAAC (Schaaf & Wang, 2021). The MODSCAG SCF data are publicly available from the Snow Data System at NASA-JPL, with the STC version available by request from NSIDC Snow Today at https://nsidc.org/snow-today (Rittger et al., 2022). Fire severity data are publicly available from MTBS at https://www.mtbs.gov/ (Eidenshink et al., 2007). Ecoregion information is available at https://www.epa.gov/eco-research/ecoregion-download-files-state-region-9 (Griffith et al., 2016). Tree cover data are available from the Multi-Resolution Land Characteristics Consortium at https://www.mrlc.gov/ (Ruefenacht et al., 2008).

Acknowledgments
This work is funded by the National Science Foundation, CNH-2 Dynamics of Integrated Socio-Environmental Systems Program, Award #2009726. Spatially and temporally complete MODIS snow fraction data provided by Karl Rittger/ Snow Today.

References

Abatzoglou, J. T., & Williams, A. P. (2016). Impact of anthropogenic climate change on wildfire across Western US forests. *Proceedings of the National Academy of Sciences*, *113*(42), 11770–11775. https://doi.org/10.1073/pnas.1607171113

Alizadeh, M. R., Abatzoglou, J. T., Luce, C. H., Adamowski, J. F., Farid, A., & Sadegh, M. (2021). Warming enabled upslope advance in Western US forest fires. *Proceedings of the National Academy of Sciences USA*, *118*(22), e2009717118. https://doi.org/10.1073/pnas.2009717118

Andrews, T., Betts, R. A., Booth, B., Jones, C. D., & Jones, G. S. (2017). Effective radiative forcing from historical land use change. *Climate Dynamics*, *10*(11–12), 3489–3505. https://doi.org/10.1007/s00382-016-3280-7

Bales, R. C., Hopmans, J. W., O'Geen, A. T., Meadows, M., Hartsough, P. C., Kirchner, P., et al. (2011). Soil moisture response to snowmelt and rainfall in a Sierra Nevada mixed-conifer forest. *Vadose Zone Journal*, *10*(3), 786–799. https://doi.org/10.2136/vzj2011.0001

Barbero, R., Abatzoglou, J., Larkin, N. K., Kolden, C. A., & Stocks, B. (2015). Climate change presents increased potential for very large fires in the contiguous United States. *International Journal of Wildland Fire*, *24*(7), 892. https://doi.org/10.1071/WF15083

Barnes, C. A., & Roy, D. P. (2010). Radiative forcing over the conterminous United States due to contemporary land cover land use change and sensitivity to snow and interannual albedo variability. *Journal of Geophysical Research*, *115*(G4), G04033. https://doi.org/10.1029/2010JG001428

Betts, R. A. (2000). Offset of the potential carbon sink from boreal forestation by decreases in surface albedo. *Nature*, *408*(6809), 187–190. https://doi.org/10.1038/35041545

Bonan, G. B., Chapin III, F. S., & Thompson, S. L. (1995). Boreal forest and tundra ecosystems as components of the climate system. *Climatic Change*, *29*(2), 145–167. https://doi.org/10.1007/bf01094014

Bonan, G. B., Pollard, D., & Thompson, S. L. (1992). Effects of boreal forest vegetation on global climate. *Nature*, *359*(6397), 716–718. https://doi.org/10.1038/359716a0

Boon, S. (2009). Snow ablation energy balance in a dead forest stand. *Hydrological Processes*, *23*(18), 2600–2610. https://doi.org/10.1002/hyp.7246

Burakowski, E. A., Ollinger, S. V., Lepine, L., Schaaf, C. B., Wang, Z., Dibb, J. E., et al. (2015). Spatial scaling of reflectance and surface Albedo over a mixed-use, temperate forest landscape during snow-covered periods. *Remote Sensing of Environment*, *158*, 465–477. https://doi.org/10.1016/j.rse.2014.11.023

Burles, K., & Boon, S. (2011). Snowmelt energy balance in a burned forest plot, Crowsnest Pass, Alberta, Canada. *Hydrological Processes*, *25*(19), 3012–3029. https://doi.org/10.1002/hyp.8067

Coulston, J., Moisen, G., Wilson, B., Finco, M., Cohen, W., & Brewer, C. (2012). Modeling percent tree canopy cover: A pilot study. *Photogrammetric Engineering and Remote Sensing*, *78*(7), 715–727. https://doi.org/10.14358/pers.78.7.715

Cox, C., Stone, R., Douglas, D., Stanitski, D., Divoky, G., Dutton, G., et al. (2017). Drivers and environmental responses to the changing annual snow cycle of Northern Alaska. *Bulletin of the American Meteorological Society*, *78*(7), 715–727. https://doi.org/10.1175/BAMS-D-16-0201.1

Dennison, P. E., Brewer, S. C., Arnold, J. D., & Moritz, M. A. (2014). Large wildfire trends in the Western United States, 1984–2011. *Geophysical Research Letters*, *41*(8), 2928–2933. https://doi.org/10.1002/2014GL059576

Eidenshink, J., Schwind, B., Brewer, K., Zhu, Z., Quayle, B., & Howard, S. (2007). A project for monitoring trends in burn severity [Dataset]. *Fire Ecology*, *3*(1), 3–21. https://doi.org/10.4996/fireecology.0301003

Euskirchen, E. S., McGuire, A. D., Rupp, T. S., Chapin, F. S., & Walsh, J. E. (2009). Projected changes in atmospheric heating due to changes in fire disturbance and the snow season in the Western Arctic, 2003–2100. *Journal of Geophysical Research*, *114*(G4), G04022. https://doi.org/10.1029/2009JG001095

French, N., Whitley, M., & Jenkins, L. (2016). Fire disturbance effects on land surface albedo in Alaskan tundra. *Journal of Geophysical Research*, *121*(3), 841–854. https://doi.org/10.1002/2015jg003177

Gergel, D. R., Nijssen, B., Abatzoglou, J. T., Lettenmaier, D. P., & Stumbaugh, M. R. (2017). Effects of climate change on snowpack and fire potential in the Western USA. *Climatic Change*, *141*(2), 287–299. https://doi.org/10.1007/s10584-017-1899-y

Gersh, M., Gleason, K., & Surunis, A. (2022). Forest fire effects on landscape snow albedo recovery and decay. *Remote Sensing*, *14*(16), 4079. https://doi.org/10.3390/rs14164079

Ghimire, B., Williams, C., Collatz, G., & Vanderhoof, M. (2012). Fire-induced carbon emissions and regrowth uptake in Western U.S. Forests: Documenting variation across forest types, fire severity, and climate regions. *Journal of Geophysical Research*, *117*(G3), G03036. https://doi.org/10.1029/2011jg001935

Gleason, K., & Nolin, A. (2016). Charred forests accelerate snow albedo decay: Parameterizing the post-fire. Radiative forcing on snow for three years following fire. *Hydrological Processes*, *30*(21), 3855–3870. https://doi.org/10.1002/hyp.10897

Gleason, K., Nolin, A., & Roth, T. (2013). Charred forests increase snowmelt: Effects of burned woody debris and incoming solar radiation on snow ablation. *Geophysical Research Letters*, *40*(17), 4654–4661. https://doi.org/10.1002/grl.50896
Gleason, K. E., McConnell, J. R., Arienzo, M. M., Chellman, N., & Calvin, W. M. (2019). Four-fold increase in solar forcing on snow in Western U.S. Burned forests since 1999. *Nature Communications*, *10*(1), 2026. https://doi.org/10.1038/s41467-019-09935-y
Griffith, G., Omernik, J., Smith, D., Cook, T., Tallyn, E., Moseley, K., & Johnson, C. (2016). Ecoregions of California (2 sided color poster with map, descriptive text, and photographs) [Dataset]. *U.S. Geological Survey Open-File Report*. 100000. https://doi.org/10.3133/ofr20161021
Gutierrez, A., Hantson, S., Langenbrunner, B., Chen, B., Jin, Y., Goulden, M., & Randerson, J. (2021). Wildfire response to changing daily temperature extremes in California's Sierra Nevada. *Science Advances*, *7*(47), eabe6417. https://doi.org/10.1126/sciadv.abe6417
Harpold, A., Biederman, J., Condon, K., Merino, M., Korgaonkar, Y., Nan, T., et al. (2013). Changes in snow accumulation and ablation following the Las Conchas Forest fire, New Mexico, USA. *Ecohydrology*, *7*(2), 440–452. https://doi.org/10.1002/eco.1363
Harpold, A., Molotch, N., Musselman, K., Bales, R., Kirchner, P., Litvak, M., & Brooks, P. (2015). Soil moisture response to snowmelt timing in mixed-conifer subalpine forests. *Hydrological Processes*, *29*(12), 2782–2798. https://doi.org/10.1002/hyp.10400
Hatchett, B. J. (2021). Seasonal and ephemeral snowpacks of the conterminous United States. *Hydrology*, *8*(1), 32. https://doi.org/10.3390/hydrology8010032
Jin, Y., & Roy, D. (2005). Fire-induced albedo change and its radiative forcing at the surface in Northern Australia. *Geophysical Research Letters*, *32*(13), L13401. https://doi.org/10.1029/2005gl022822
Kampf, S. K., Mcgrath, D., Sears, M. G., Fassnacht, S. R., Kiewiet, L., & Hammond, J. C. (2022). Increasing wildfire impacts on snowpack in the Western U.S. *Proceedings of the National Academy of Sciences*, *119*(39), e2200333119. https://doi.org/10.1073/pnas.2200333119
Key, C., & Benson, N. (2005). Landscape assessment: Remove sensing of severity, the normalized burn ratio. In D. C. Lutes (Ed.), *Firemon: Fire effects monitoring and inventory system. General Technical Report, RMRS-GTR-164-CD:LA1-LA51 (pp)*. USDA Forest Service, Rocky Mountain Research Station.
Koshkin, A., Hatchett, B., & Nolin, A. (2022). Wildfire impacts on Western United States snowpacks. *Frontiers in Water*, *4*, 971271. https://doi.org/10.3389/frwa.2022.971271
Li, D., Wrzesien, M. L., Durand, M., Adam, J., & Lettenmaier, D. P. (2017). How much runoff originates as snow in the Western United States, and how will that change in the future? *Geophysical Research Letters*, *44*(12), 6163–6172. https://doi.org/10.1002/2017GL073551
Li, R., Wang, D., Wang, W., & Nemani, R. (2022). A GeoNEX-based high-spatiotemporal-resolution product of land surface downward shortwave radiation and photosynthetically active radiation. *Earth System Science Data*, *15*(3), 1419–1436. https://doi.org/10.5194/essd-15-1419-2023
Littell, J. S., McKenzie, D., Peterson, D. L., & Westerling, A. L. (2009). Climate and wildfire area burned in Western U.S. Ecoprovinces, 1916–2003. *Ecological Applications*, *19*(4), 1003–1021. https://doi.org/10.1890/07-1183.1
Liu, H., Randerson, J. T., Lindfors, J., & Chapin III, F. S. (2005). Changes in the surface energy budget after fire in boreal ecosystems of interior Alaska: An annual perspective. *Journal of Geophysical Research*, *110*(D13), D13101. https://doi.org/10.1029/2004JD005158
McGrath, D., Zeller, L., Bonnell, R., Reis, W., Kampf, S., Williams, K., et al. (2023). Declines in peak snow water equivalent and elevated snowmelt rates following the 2020 Cameron Peak wildfire in Northern Colorado. *Geophysical Research Letters*, *50*(6), e2022GL101294. https://doi.org/10.1029/2022GL101294
Micheletty, P. D., Kinoshita, A. M., & Hogue, T. S. (2014). Application of MODIS snow cover products: Wildfire impacts on snow and melt in the Sierra Nevada. *Hydrological Earth Systems Science*, *18*(11), 4601–4615. https://doi.org/10.5194/hess-18-4601-2014
Miller, C., & Urban, D. L. (1999). A model of surface fire, climate and forest pattern in the Sierra Nevada, California. *Ecological Modelling*, *114*(2–3), 113–135. https://doi.org/10.1016/S0304-3800(98)00119-7
Miller, J., & Thode, A. (2007). Quantifying burn severity in a heterogeneous landscape with a relative version of the delta Normalized Burn Ratio (RdNBR). *Remote Sensing of Environment*, *109*(1), 66–80. https://doi.org/10.1016/j.rse.2006.12.006
Morgan, P., Heyerdahl, E. K., & Gibson, C. E. (2008). Multi-season climate synchronized forest fires throughout the 20th century, Northern Rockies, USA. *Ecology*, *89*(3), 717–728. https://doi.org/10.1890/06-2049.1
Painter, T., Rittger, K., Mckenzie, C., Slaughter, P., Davis, R., & Dozier, J. (2009). Retrieval of subpixel snow covered area, grain size, and albedo from MODIS. *Remote Sensing of Environment*, *113*(4), 868–879. https://doi.org/10.1016/j.rse.2009.01.001
Pielke, R., Pitman, A., Niyogi, D., Mahmood, R., McAlpine, C., Hossain, F., et al. (2011). Land use/land cover changes and climate: Modeling analysis and observational evidence. *WIREs Climate Change*, *2*(6), 828–850. https://doi.org/10.1002/wcc.144
Pomeroy, J., & Dion, K. (1996). Winter radiation extinction and reflection in a boreal pine canopy: Measurements and modelling. *Hydrological Processes*, *10*(12), 1591–1608. https://doi.org/10.1002/(SICI)1099-1085(199612)10:12<1591::AID-HYP503>3.0.CO;2-8
Rittger, K., Bormann, K. J., Bair, E. H., Dozier, J., & Painter, T. H. (2021). Evaluation of VIIRS and MODIS snow cover fraction in high-mountain Asia using Landsat 8 OLI. *Frontiers in Remote Sensing*, *2*, 647154. https://doi.org/10.3389/frsen.2021.647154
Rittger, K., Brodzik, M. J., & Raleigh, M. (2022). Snow today [Dataset]. *National Snow and Ice Data Center*. https://nsidc.org/snow-today/
Rittger, K., Raleigh, M., Dozier, J., Hill, A., Lutz, J., & Painter, T. (2020). Canopy adjustment and improved cloud detection for remotely sensed snow cover mapping. *Water Resources Research*, *56*(6), e2019WR024914. https://doi.org/10.1029/2019wr024914
Robinson, D. A., & Kukla, G. (1984). Albedo of a Dissipating snow cover. *Journal of Applied Meteorology and Climatology*, *23*(12), 1626–1634. https://doi.org/10.1175/1520-0450(1984)023<1626:AOADSC>2.0.CO;2
Rother, D., & De Sales, F. (2021). Impact of wildfire on the surface energy balance in six California case studies. *Boundary-Layer Meteorology*, *178*(1), 143–166. https://doi.org/10.1007/s10546-020-00562-5
Rother, D., De Sales, F., Stow, D., & McFadden, J. (2022). Impacts of burn severity on short-term postfire vegetation recovery, surface albedo, and land surface temperature in California ecoregions. *PLoS One*, *17*(11), e0274428. https://doi.org/10.1371/journal.pone.0274428
Ruefenacht, B., Finco, M., Nelson, M., Czaplewski, R., Helmer, E., Blackard, J., et al. (2008). Conterminous U.S. and Alaska forest type mapping using forest inventory and analysis data [Dataset]. *Photogrammetric Engineering and Remote Sensing*, *74*(11), 1379–1388. https://doi.org/10.14358/PERS.74.11.1379
Schaaf, C., & Wang, Z. (2021). MODIS/Terra+Aqua BRDF/Albedo daily L3 global - 500m V061 [Dataset]. *NASA EOSDIS Land Processes Distributed Active Archive Center*. https://doi.org/10.5067/MODIS/MCD43A3.061
Schwartz, M., Butt, N., Dolanc, C., Holguin, A., Moritz, M., North, M., et al. (2015). Increasing elevation of fire in the Sierra Nevada and implications for forest change. *Ecosphere*, *6*(7), 121–210. https://doi.org/10.1890/ES15-00003.1
Shrestha, S., Williams, C., Rogers, B., Rogan, J., & Kulakowski, D. (2022). Wildfire controls on land surface properties in mixed conifer and ponderosa pine forests of Sierra Nevada and Klamath mountains, Western. *US.Agricultural and Forest Meteorology*, *320*, 108939. https://doi.org/10.1016/j.agrformet.2022.108939
Stillinger, T., Rittger, K., Raleigh, M. S., Michell, A., Davis, R. E., & Bair, E. H. (2023). Landsat, MODIS, and VIIRS snow cover mapping algorithm performance as validated by airborne lidar datasets. *The Cryosphere*, *17*(2), 567–590. https://doi.org/10.5194/tc-17-567-2023

Stone, R. S., Dutton, E. G., Harris, J. M., & Longenecker, D. (2002). Earlier spring snowmelt in Northern Alaska as an indicator of climate change. *Journal of Geophysical Research*, *107*(D10), ACL10. https://doi.org/10.1029/2000JD000286

Uecker, T. M., Kaspari, S. D., Musselman, K. N., & Skiles, S. M. (2020). The post-wildfire impact of burn severity and age on black carbon snow deposition and implications for snow water resources, cascade range, Washington. *Journal of Hydrometeorology*, *21*(8), 1777–1792. https://doi.org/10.1175/jhm-d-20-0010.1

Veraverbeke, S., Verstraeten, W. W., Lhermitte, S., Van de Kerchove, R., & Goossens, R. (2012). Assessment of post-fire changes in land surface temperature and surface albedo, and their relation with fire-burn severity using multitemporal MODIS imagery. *International Journal of Wildland Fire*, *21*(3), 243–256. https://doi.org/10.1071/wf10075

Vlassova, L., Pérez-Cabello, F., Mimbrero, M. R., Llovería, R. M., & García-Martín, A. (2014). Analysis of the relationship between land surface temperature and wildfire severity in a series of Landsat images. *Remote Sensing*, *6*(7), 6136–6162. https://doi.org/10.3390/rs6076136

Westerling, A., Bryant, B., Preisler, H., Holmes, T., Hidalgo, H., Das, T., & Shrestha, S. (2011). Climate change and growth scenarios for California wildfire. *Climatic Change*, *109*(S1), 445–463. https://doi.org/10.1007/s10584-011-0329-9

Westerling, A., Hidalgo, H., Cayan, D., & Swetnam, T. (2006). Warming and earlier spring increase Western US forest wildfire activity. *Science*, *313*(5789), 940–943. https://doi.org/10.1126/science.1128834

Westerling, A. L. R. (2016). Increasing western US forest wildfire activity: Sensitivity to changes in the timing of spring. *Philosophical Transactions of the Royal Society B: Biological Sciences*, *371*(1696), 1–10. https://doi.org/10.1098/rstb.2015.0178

Williams, A. P., & Abatzoglou, J. T. (2016). Recent advances and remaining uncertainties in resolving past and future climate effects on global fire activity. *Current Climate Change Reports*, *2*(1), 1–14. https://doi.org/10.1007/s40641-016-0031-0

Williams, A. P., Abatzoglou, J. T., Gershunov, A., Guzman-Morales, J., Bishop, D. A., Balch, J. K., & Lettenmaier, D. P. (2019). Observed impacts of anthropogenic climate change on wildfire in California. *Earth's Future*, *7*(8), 892–910. https://doi.org/10.1029/2019EF001210

Williams, A. P., Livneh, B., McKinnon, K. A., Hansen, W. D., Mankin, J. S., Cook, B. I., et al. (2022). Growing impact of wildfire on western US water supply. *Proceedings of the National Academy of Sciences*, *119*(10), e2114069119. https://doi.org/10.1073/pnas.2114069119

Winkler, R. (2011). Changes in snow accumulation and ablation after a fire in South-Central British Columbia. *Streamline Watershed Management Bulletin*, *14*, 1–7.

Wiscombe, W., & Warren, S. (1980). A model for the spectral albedo of snow. I: Pure snow. *Journal of the Atmospheric Sciences*, *37*(12), 2712–2733. https://doi.org/10.1175/1520-0469(1980)037<2712:AMFTSA>2.0.CO;2